Available online at www.sciencedirect.com
ScienceDirect
Acta Materialia 57 (2009) 6047–6056
Acta MATERIALIA
www.elsevier.com/locate/actamat

Nucleation and growth of twins in Zr: A statistical study

L. Capolungo, P.E. Marshall, R.J. McCabe, I.J. Beyerlein *, C.N. Tomé

Materials Science and Technology Division, Los Alamos National Laboratory, Los Alamos, NM 87545, USA
Theoretical Division, Los Alamos National Laboratory, Los Alamos, NM 87545, USA

Received 29 April 2009; received in revised form 12 August 2009; accepted 14 August 2009
Available online 18 September 2009

Abstract

An in-depth statistical analysis using electron backscatter diffraction (EBSD) is carried out to expose statistical correlations between $\{10\bar{1}2\}$ twinning and grain size, crystallographic orientation, grain boundary length, and neighbor misorientation in high-purity polycrystalline zirconium strained to 5% and 10% at 77 K. A strong correlation was found between the active twin variant and crystallographic orientation. The propensity of a grain to twin or not was found to be only weakly dependent on grain area and diameter. Within the population of grains containing twins the number of twins per grain noticeably increases with grain area, and twin thickness is found to be rather insensitive to grain size and orientation. A weak preference for twinning was found for smaller grain boundary misorientation angles. These and the other statistical results reported can improve theoretical treatments for twin nucleation in polycrystal models. The statistical methodology presented has general applicability for all twin types in a wide range of metals.

Keywords: Twinning; Statistics; Grain size; EBSD; Zirconium

1. Introduction

Twinning is an important deformation mode in high-purity, hexagonal close packed (hcp) polycrystalline zirconium (Zr) at room temperature and below [1–6]. In hcp metals (e.g., Zr, Mg, Hf, Ti, Be), the $\{10\bar{1}2\}$ twinning mode is the most commonly observed twin type [5,6]. In those metals with c/a ratios below $\sqrt{8/3}$, such as Zr, the $\{10\bar{1}2\}$ twin is referred to as a tensile twin because it forms when the c-axis of a grain is loaded in tension [7–9]. Both slip and twinning are inelastic deformation mechanisms that control the plastic anisotropic response of zirconium. However, unlike slip, twinning provides shear strain via re-orientation of the lattice. This can have a dramatic effect on the flow stress and work hardening rate of a material due to a re-orientation of material to a "softer" orientation, as is the case for the $\{11\bar{2}2\}$ compressive twin, or a re-orientation to a "harder" orientation, as is the case for the $\{10\bar{1}2\}$ tensile twin [3]. The introduction of twin boundaries can also affect the flow stress and hardening, by interacting with the dislocations presently active in the grain. To date, much progress has been made in several studies at various length scales regarding the effects of twinning on the constitutive response of hcp metals, and the interactions between twinning and slip [3,4,6,10–17]. There are, however, many questions concerning twin nucleation and twin propagation that remain unanswered.

To shed some light on the relevant micro-scale features responsible for twin nucleation and growth, we conducted an experimentally based statistical analysis of deformation twinning in zirconium. Strongly textured polycrystalline Zr samples were strained to 5% and 10% at 77 K in an orientation that favors activation of $\{10\bar{1}2\}$ tensile twins. Large statistical sample sizes were analyzed using electron backscatter diffraction (EBSD), and data were collected on grain size, grain orientation, grain boundary length, grain boundary misorientation angle, twin thickness, twin variant, etc. The analysis revealed which microstructural features are strongly correlated with certain characteristics of twin nucleation or twin growth and which are not.

* Corresponding author. Address: Theoretical Division, Los Alamos National Laboratory, Los Alamos, NM 87545, USA.
E-mail address: Irene@lanl.gov (I.J. Beyerlein).

1359-6454/$36.00 © 2009 Acta Materialia Inc. Published by Elsevier Ltd. All rights reserved.
doi:10.1016/j.actamat.2009.08.030

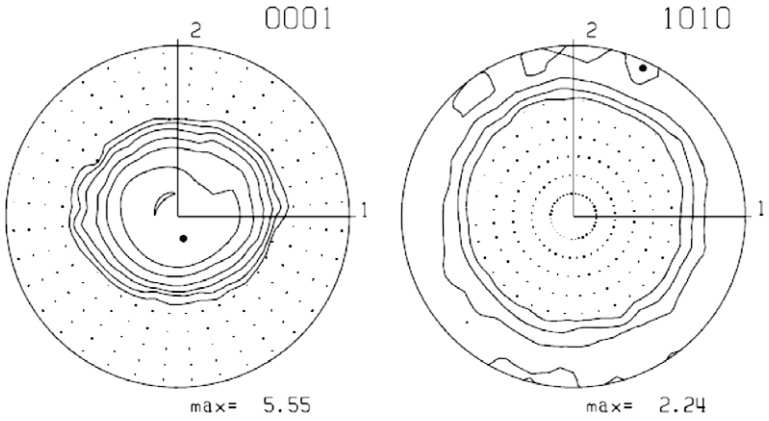

Fig. 1. Basal (0 0 0 1) and prism (10$\bar{1}$0) pole figures of the clock-rolled high-purity zirconium studied in this work. The 3-axis is the through-thickness direction of the plate. Contour levels: 0.7/1.0/1.4/2.0/2.83/4.0.

Although such correlations are empirical and we can only speculate about the physical mechanisms responsible for them, we believe this approach will help in the development of probabilistic twinning models that can be incorporated into polycrystal plasticity models. Currently, such polycrystal models deal with twinning in a deterministic way, although it is known that twinning is of a statistical nature and depends strongly on local conditions inside grains and at grain boundaries.

2. Experimental procedure and statistical treatment

High-purity crystal bar Zr (<100 ppm) was arc-melted, cast into an ingot, and clock-rolled at room temperature, where clock rolling refers to a rolling schedule involving a rotation of the plate between rolling passes [3]. Compression specimens were machined from the plate and annealed at 550 °C for 1 h resulting in twin-free, equi-axed grains with an average grain size of approximately 17 μm. As shown in Fig. 1, the final product has a strong axisymmetric texture with the basal poles aligned within approximately 30° of the through-thickness direction (3-axis). Samples were loaded in compression in one of the in-plane directions of the plate (IPC) at 77 K to induce {10$\bar{1}$2} twinning.

Automated EBSD quantitative analysis [16] using 0.2 μm step size was used to obtain statistical data on several features of the grains, twins, and grain boundaries for samples loaded to 5% and 10% strain. The corresponding stresses at these strains were 270 MPa and 370 MPa. Data were collected from four and six distinct 120 × 240 μm scans at different locations on the same cross section of the 5% and 10% samples, respectively. A typical scan from each sample is shown in Fig. 2. Statistical variations in twin morphology and area fraction across the scan and from grain to grain are evident. The primary twin type found is the {10$\bar{1}$2} twin and is the focus of the present analysis, however there were also a relatively small number of {11$\bar{2}$1} twins.

Each grain is marked either as an un-twinned grain or twinned grain, where a twinned grain contains at least one visible twin with some grains containing more than one set of twin variants. A few grains contain twins that

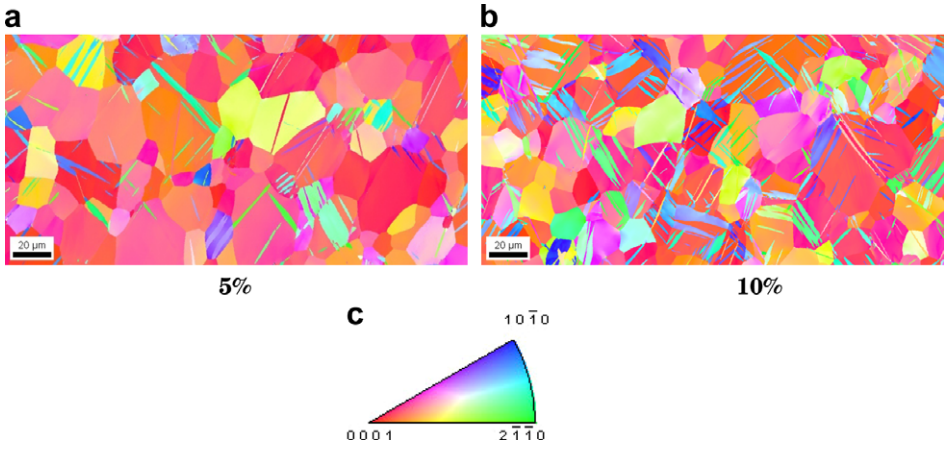

Fig. 2. Example EBSD scans for specimens loaded in in-plane compression to: (a) 5% strain, and (b) 10% strain. The sections shown correspond to the rolling plane, and the compressive direction is horizontal to the figure. The orientation key is shown in (c) as an inverse pole figure of the normal to the rolling plane.

Table 1
Size of statistical data sets obtained from the set of EBSD scans for each strain level. Twins refer to the $\{10\bar{1}2\}$ type. Small grains with a confidence index less than 0.1 are excluded from the analysis.

	5% Strain	10% Strain
Number of grains N_g	349	639
Number of twinned grains N_{tg}	201	462
Number of twins N_{tw}	~405	~1065
Number of grain boundaries N_{gb}	1121	2043
Total twin area fraction A	5%	16%

did not propagate across the grain within the EBSD scan plane. All twins are included in the statistical analysis. Table 1 lists the sizes of the data sets examined: the total number of grains N_g, twinned grains N_{tg}, twins N_{tw}, and grain boundaries N_{gb}. The last entry in Table 1 shows that the total twin area fraction A_{tw} increases from 5% to 16%. Hereinafter, upper case letters are used to identify quantities that are calculated by summing over the entire scanned area.

A statistical analysis was then performed on the EBSD data to identify possible relationships between twinning and other microstructural features. For each grain, the area a_g is calculated including the area of any twinned regions. For each twinned grain, the number of twins n, the twin variant v, twin thickness w, twinned area a_t, and twin area fraction a_f are determined. For grains containing more than one twin variant, the twinned area in that grain considers only the twinned area corresponding to the variant of the largest twin in that grain. Grain area and twin area are measurements based on an EBSD scan of a 2D section of the material. Because the grains are relatively equi-axed, grain area is a good measure of grain size. As for twin area, the true twin thicknesses was estimated by multiplying the measured thickness by $\cos\theta$, where θ is the angle between twin plane normal, K_1, and the normal to the sample. Lower case letters are used to emphasize that these quantities are calculated per grain.

We characterized the grain boundaries by the misorientation angle α. Given two adjoining grains A and B sharing a single boundary, the misorientation angle α across this boundary is defined by:

$$\alpha = \min\left[\cos^{-1}\left(\frac{tr(R_A R_B^T)-1}{2}\right)\right] \quad (1)$$

where R_A and R_B denote the rotation matrices that transform from the crystal axes of grains A and B to the sample axes. Because of crystal symmetry, the same orientation can be achieved by different sets of R. As indicated in Eq. (1), α is defined by the minimum over all possibilities. We use a 5° tolerance angle to identify grain boundaries in our automated EBSD analysis, and thus, this represents the minimum possible α.

Both twin nucleation and twin propagation are analyzed from a statistical viewpoint. For this analysis we associate each observed twin lamella with a successful nucleation event. The statistics concerning twin nucleation as a function of the measured microstructure are based on the entire population of grains. The statistics concerning twin growth are based only on the subset of grains containing twins, and include the average thickness of the twins w in a twinned grain, the twin area a_t, and the twin area fraction a_f. The nucleation part of the analysis is not concerned with these features.

The data will be presented in histograms, which plot a statistical quantity versus a given parameter. The parameter space is divided into equal-sized bins. The bin size is selected specifically for each plot such that it is not so large that variations are lost but not too small that any one bin contains less than five data points. In most cases, the same conclusions apply to both the 5% and 10% samples and so, unless stated otherwise, data reported hereinafter correspond to the 10%-strained sample.

3. Orientation effects on twinning

We take advantage of the macroscopic axial stress state to employ a Schmid factor analysis to examine the relationship between deformation twinning and the crystallographic orientation of each grain. For each twin, a geometric Schmid factor is calculated as the ratio of the shear stress resolved on the twin plane and along the twin shear direction over the applied macroscopic compressive stress. Experimentally we are only able to define a geometric Schmid factor and cannot measure the resolved shear stress in the twin plane. The local stress tensor in the grain does not, in general, coincide with the applied stress and, therefore, the actual resolved shear stress may not be equal to the product of the geometric Schmid factor and the applied stress. Although not shown, it is found that grain orientation is uncorrelated with grain size. Therefore, in what follows, orientation effects and size effects can be studied independently.

3.1. Effect on twin nucleation

Fig. 3 represents the propensity of a grain of a given orientation to twin. Based on the orientation of each grain (or 'parent' in the case of a twinned grain) the highest twin Schmid factor among the six twin variants, denoted as $m_{(1)}$, is identified. The propensity for a grain with a given $m_{(1)}$ to twin is represented by the number of grains within an interval of $m_{(1)}$ that have at least one twin divided by the total number of grains within the same interval. As expected, twin activation occurs preferentially in grains favorably oriented for twinning, e.g., $m_{(1)} > 0.37$. The analysis in Fig. 3, however, shows two rather unexpected results. First, some grains twinned that would not usually be considered oriented for twinning, e.g., $m_{(1)} < 0.25$. Second, not all grains with the same $m_{(1)}$ (within a given interval) responded in the same way: 10% did not twin at the highest Schmid factors ($m_{(1)} > 0.37$). These observations strongly point to the local nature of twin nucleation because (a) nucleation occurs both in grains favorably ori-

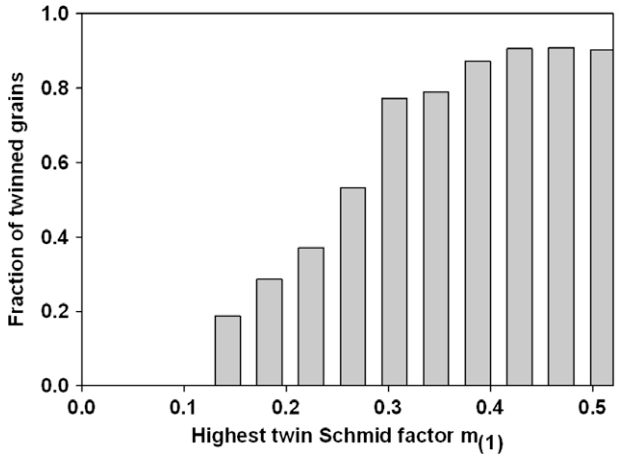

Fig. 3. Data showing that the fraction of twinned grains (that contained at least one twin) increases with $m_{(1)}$, the highest Schmid factor among the six twin variants in each grain. $m_{(1)}$ is calculated based on the orientation of the parent grain.

ented and not so favorably oriented for twinning and (b) twins appear only in a fraction of the grains that are favorably oriented for twinning.

3.2. Effect of prismatic slip

Our previous studies on Zr [2,3,17] have shown that twinning is preceded by and operates with prismatic slip during IPC deformation at 77 K. In this strongly textured material, most of the grains are oriented well for both slip and tensile twinning. For the texture and IPC loading considered here, the difference between the highest Schmid factors on the twin and prismatic slip systems $m_{(1)}^{\text{twin}} - m_{(1)}^{\text{prism}}$ is very small, less than 0.05 for nearly all of the orientations represented by the initial texture (very few orientations had their c-axis aligned with the compressive direction in this particular texture). Also, with respect to accommodating deformation, the primary difference between these two mechanisms is that $\{10\bar{1}2\}$ twinning results in an elongation approximately parallel to the c-axis direction and prismatic slip results in an elongation perpendicular to the c-axis and compressive loading direction. It seems, however, that $\{10\bar{1}2\}$ twinning and prismatic slip accommodate compressive strain nearly equally well for compression at high angles (roughly perpendicular) to the c-axis. Accordingly, in order for a crystal to expand in all directions in response to a compressive loading perpendicular to its c-axis, it is necessary for both of these mechanisms to be active. For these reasons, it is likely that prismatic slip and tensile twinning are both active in most orientations, even though their threshold stresses are different.

Also, it has been proposed that prismatic slip dislocations could help twin nucleation [18–20] or twin growth [11,21]. However, it can also be argued that prismatic slip dislocations could hinder these processes [22]. Using the current statistical approach, we explored possible correlations between prismatic slip activity, quantified by the Schmid factor of the prismatic slip systems, and deformation twinning. No correlations were found between the propensity for twin formation or twin growth with the Schmid factors for prismatic slip, either in the same grain or in the neighboring grains. This result may imply that prior slip, or more specifically slip dissociations or slip dislocation pile-ups, are not a prerequisite for twin nucleation. This is consistent with stability calculations in [18] which showed that a pile-up of prismatic slip dislocations, regardless of its size, cannot lead to the formation of stable twin faults on the $\{10\bar{1}2\}$ twin plane. Regarding twin growth, this supports the conclusions from a recent study [13] on this same Zr material, that stored prismatic dislocations generated in IPC at 300 K do not hinder twin growth during subsequent IPC loading at 77 K. It is also consistent with the conclusion in [11] that reactions between $\langle a \rangle$ type dislocations and $\{10\bar{1}2\}$ twin boundaries are not the primary mechanisms for twin thickening (growth transverse to the twin plane). Nonetheless, this result motivates a deeper look, both theoretically and experimentally, at dislocation activity in the region of the twin.

3.3. Twin variant selection

In this section, we compare the Schmid factor corresponding to each observed twin in the grain with the Schmid factor of those other twin variants that did not appear. For the former, Fig. 4 shows the distribution of Schmid factors on the population of observed twins. As shown, more twins are found with higher Schmid factors. This trend is not surprising. Because of the strong texture with respect to the applied loading, there are many grains with high twin Schmid factors and, consequently, the Schmid factors for the twins that nucleated is likely to be high. The more interesting aspect to note is the wide dispersion in these Schmid factors. The median Schmid factor is 0.37, meaning that half the twins had a Schmid factor greater than 0.37.

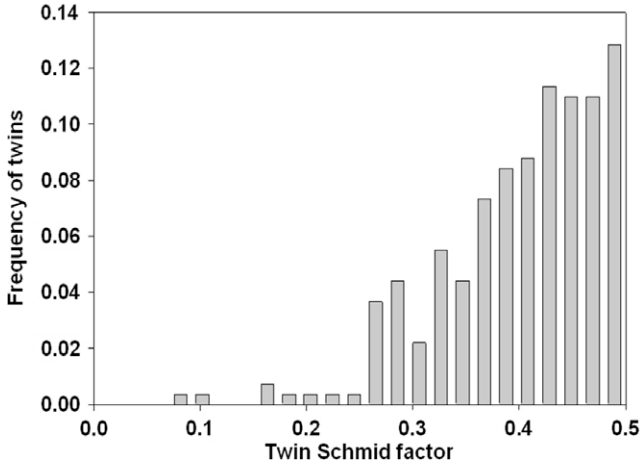

Fig. 4. The distribution of Schmid factor on the observed twins.

The average frequency for each variant is summarized in Table 2. The six possible twin variants in each grain ($v_{(i)}$, $i = 1, 6$) are classified in order of decreasing Schmid factor. Accordingly, the first variant $v_{(1)}$ has the highest Schmid factor $m_{(1)}$, the second $v_{(2)}$, the second highest $m_{(2)}$, and the sixth $v_{(6)}$, the lowest $m_{(6)}$. From the data in Table 2, we observe that while a majority of the twins activated are $v_{(1)}$, $v_{(1)}$ is not always the variant selected. For both strain levels, the likelihood that the nucleated twin corresponds to the first variant decreases with its Schmid factor, and the possibility of nucleating variants $v_{(2)}$, $v_{(3)}$, or $v_{(4)}$ is non-negligible. The frequency of each variant is more or less the same in the 5% and 10% strained material.

For a more refined view of twin variant activation, Fig. 5a compares the Schmid factor of the active twin variant normalized by the highest twin Schmid factor in the parent grain, $m_{(1)}$, for the 10% strained sample. In this figure, each point represents a single twin occurrence and the different symbols (colors) indicate the active twin variant. (The reason that all of the $v_{(1)}$ points do not lie exactly at $m_{(i)}/m_{(1)} = 1.0$, and on occasion $v_{(2)}$ points are above 1.0, is due to subsequent slip deformation in the parent and/or twin that causes the misorientation between the parent and twin and thus the twin Schmid factor to deviate from the ideal twin misorientation.) As shown, most twins lie in the range $0.3 < m_{(1)} < 0.5$ where, surprisingly, variants of all ranks are observed, not just $v_{(1)}$ and $v_{(2)}$. As an extreme example, we find that even in grains where $0.4 < m_{(1)} < 0.5$, twins of the lower variants $v_{(5)}$ and $v_{(6)}$ are observed (see lower right-hand side).

The fact that half of the twins observed had Schmid factors below 0.37 (Fig. 4) and the observed selection of lower ranked variants, such as $v_{(2)}$ and $v_{(3)}$ (Fig. 5a) can be attributed to: (i) a deviation in the average grain stress state from the bulk stress state as a result of differences in plastic response between a grain and its neighbors, and (ii) local stress fluctuations within the grain produced by defects, dislocations, grain boundaries, and triple junctions. Furthermore, the stress variations need not be significant to nucleate twin variants of lower rank, i.e., $v_{(i)}$, $i = 2,\ldots, 6$. The difference between $m_{(1)}$ and $m_{(2)}$, for instance, is at most 0.083. To elucidate this point, the frequency of each variant is plotted in Fig. 5b as a function of its Schmid factor divided by $m_{(1)}$ of its parent grain. The occurrences of lower rank variants, such as $v_{(2)}$ and $v_{(3)}$, increase as their Schmid factor draws closer to $m_{(1)}$.

As grains become less favorably oriented for twinning these stress variations can become even more influential in variant selection. For instance when the Schmid factor on $v_{(1)}$ is 0.37, it is 0.27 on $v_{(3)}$. Considering this fact along with the results in Fig. 5, it is not too surprising that the twin variant nucleated is not always $v_{(1)}$, the one with the highest Schmid factor. The variants that are activated in the grains in a polycrystal will determine crystallographic re-orientation and, therefore, texture evolution during deformation.

Table 2
Number fraction of $\{10\bar{1}2\}$ twins of each variant found in the 5% and 10% strained samples. Fractions less than 0.01 are given a value of 0.

Strain level (%)	$v_{(1)}$	$v_{(2)}$	$v_{(3)}$	$v_{(4)}$	$v_{(5)}$	$v_{(6)}$
5	0.56	0.23	0.12	0.05	0.01	0
10	0.60	0.21	0.10	0.05	0	0

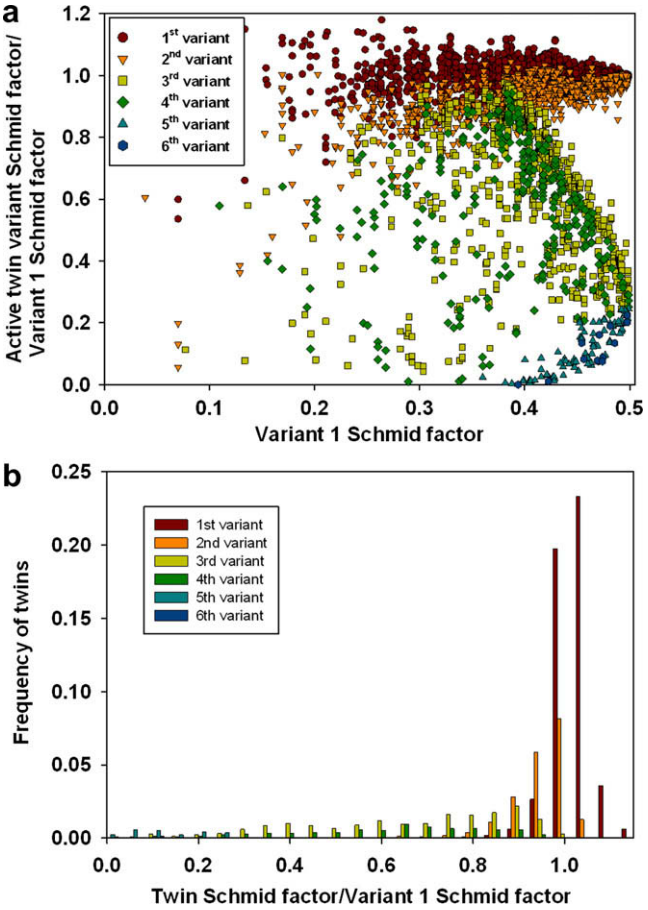

Fig. 5. (a) Comparison of the twin Schmid factor on the active twin variant normalized by the highest twin Schmid factor $m_{(1)}$ in the parent as a function of $m_{(1)}$ and (b) frequency of each variant as a function of its Schmid factor normalized by $m_{(1)}$. (The reason that all of the $v_{(1)}$ points do not lie exactly at $m_{(i)}/m_{(1)} = 1.0$, and on occasion $v_{(2)}$ points are above 1.0, is due to subsequent slip deformation in the parent and/or twin that causes the misorientation between the parent and twin and thus the twin Schmid factor to deviate from the ideal twin misorientation.)

3.4. Effect on twin growth

Fig. 6 presents the thickness per twin lamella w as a function of its corresponding m for both the 5% and 10% strained sample. The data show that above $m = 0.2$, twin thickness increases with strain. In the 5% strained sample, w is statistically constant for all m. In the 10% strained sample, as m exceeds 0.15, w exhibits a statistically significant, though small, increase with m, indicating that higher resolved shear stresses result in thicker twins.

Also for the 10% strained sample, Fig. 7 plots the twin area fraction a_f in the twinned grains as a function of the Schmid factor of the observed twin, m. It can be seen that

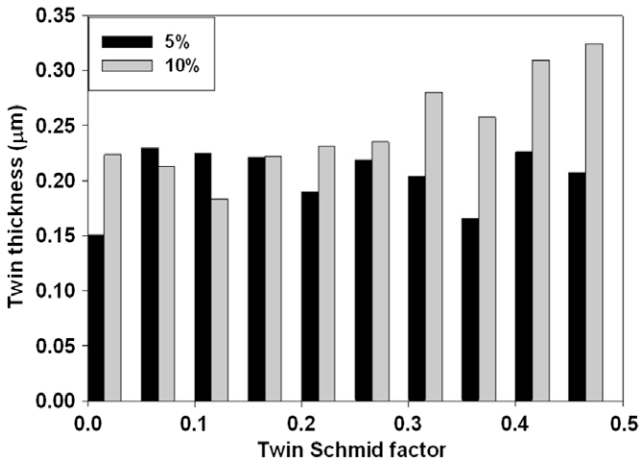

Fig. 6. Variation in the average twin thickness per twinned grain with Schmid factor on the twin for the 5% and 10% strained samples.

a_f increases moderately with m. The twin area fraction is $a_f \sim nw/d_g$, where n is the number of twins per grain and d_g is the grain diameter. As we will show later, the result in Fig. 7 is consistent with the fact that, within the twinned grains, n increases proportionally with d_g. Therefore the dependence of a_f with m follows that of w, which is also weak, as seen in Fig. 6 for this case.

4. Effects of grain boundary misorientation angle

The effect of local grain neighborhood was also explored via grain boundary misorientation angle, α. Fig. 8a shows the distribution in α across the 10% strained sample. To emphasize its deviation from random, a misorientation distribution for a non-textured hcp polycrystal is superimposed (see dashed curve). In contrast to a random texture, most of the misorientation angles in this strong texture are low.

To analyze the effect of α on twin nucleation, we calculated the number of grain boundaries with misorientation α that have at least one twin connected to it divided by the total number of boundaries with misorientation α. As shown in Fig. 8b we found a weak dependence on α, where the preference for twinning gradually decreases as α increases. However, the reader should be aware that the twin observed at the intersection with the grain boundary in the EBSD section, may have propagated from a boundary that does not appear in the section.

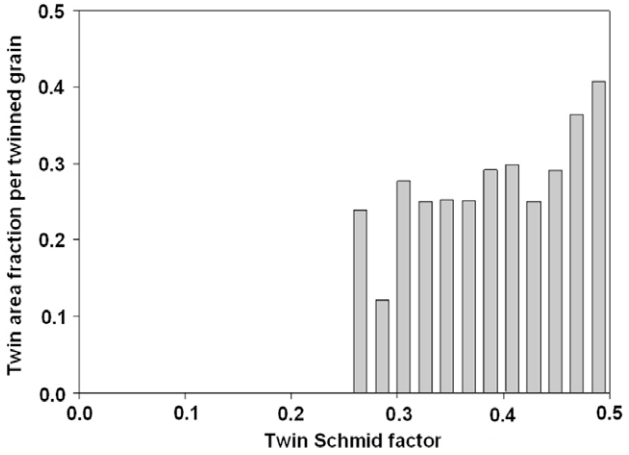

Fig. 7. The twin area fraction in the twinned grains as a function of the Schmid factor associated with the observed twin in each grain.

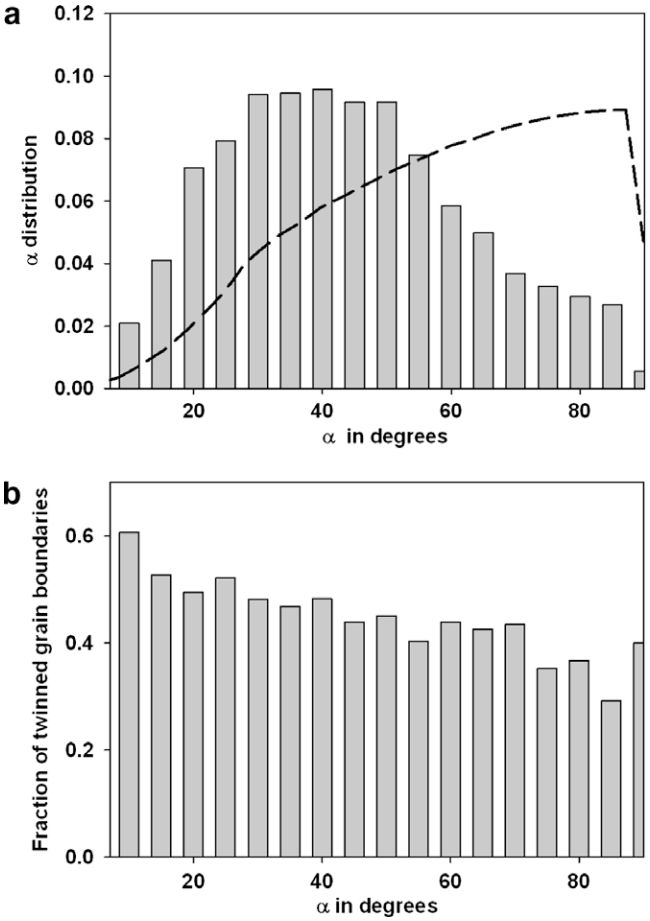

Fig. 8. (a) Distribution of misorientation angles across boundaries taken from the EBSD scans of the 10% strained material. The dashed curve represents the same distribution in a sample with no (random) texture. Because of the strong texture, there is a higher frequency of low misorientation angle boundaries than that for a random texture. (b) Fraction of twinned grain boundaries of a given misorientation angle α is found to slightly decrease with α.

5. Size effects

A positive grain size dependence of twinning has been reported in several metals, not only hcp [23–30]. It is usually found that twins appear more frequently in samples with higher average grain sizes, but it is not known if this size effect is connected with twin nucleation or twin growth. While most often the relationship is reported qualitatively, the dependence has been quantified in some cases by calculating a Hall–Petch coefficient for twinning based on a macroscopic yield stress [23–25,27,29,30] where it is

found to be an order of magnitude greater than slip. It has been argued in Ref. [31] that twinning is energetically unfavorable in smaller grains because the twin boundary energy cost relative to the plastic work done by the twin is high. Barnett [32] suggested, considering the importance of grain boundaries on twin nucleation and assuming a constant number of twins per unit of grain boundary, that the size effect is related to a decrease in the number of twins per grain with decreases in grain size.

For studying size effects on deformation twinning we investigate the grain area a_g and the related grain size d_g defined by $d_g = \sqrt{\frac{4}{\pi} a_g}$. Fig. 9a and b presents the frequency distributions for a_g and d_g found in the 10% strained sample. The grain area is observed to vary widely across the sample: approximately 50% of the grains have an area smaller than 160 μm^2 and 90% have an area smaller than 320 μm^2. Due to their small occurrences, data for grains with areas greater than 500 μm^2 are disregarded. The distribution for a_g in Fig. 9a can be described by means of an exponential distribution, whose cumulative distribution function is:

$$P(a_g < a) = 1 - \exp(-a/\alpha) \quad (2)$$

where $\alpha = 192.2\ \mu m^2$. Because $d_g = \sqrt{\frac{4}{\pi} a_g}$, the cumulative distribution for d_g in Fig. 9b is Weibull with shape parameter = 2 as follows:

$$P(d_g < d) = 1 - \exp(-(d/\delta)^2) \quad (3)$$

The scale parameter $\delta = 15.6\ \mu m$.

To reveal size effects on twin nucleation, in Fig. 10 we show the conditional probability of twinning for a given: (a) grain area a_g and (b) grain diameter d_g. In Fig. 10a, the fraction of grains that contain at least one twin and have a given a_g is plotted as a function of a_g. This plot suggests that the likelihood that twins nucleate in a grain is weakly dependent on its area a_g. Likewise, the fraction of grains twinned increases slightly with d_g. Thus, both 1D and 2D measures of grain size produce similar results.

A grain area effect is observed when considering only grains containing twins. Analysis of the twinned grain population shows that a_g is correlated with the number of twins that form per twinned grain. Fig. 11 shows that the number of twins per twinned grain of area a_g increases with a_g. Therefore, more twins are found in larger grains, provided that they twinned in the first place.

Considering again just the twinned grains, we investigate possible effects of size on twin growth. Fig. 12a and b show

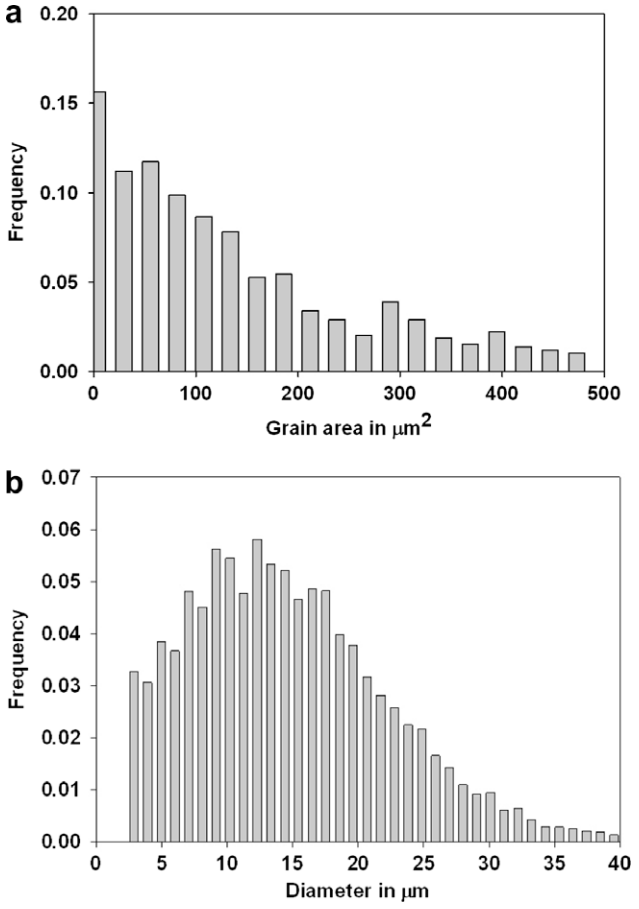

Fig. 9. Frequency distributions of: (a) grain area and (b) grain diameter in the 10% strained sample.

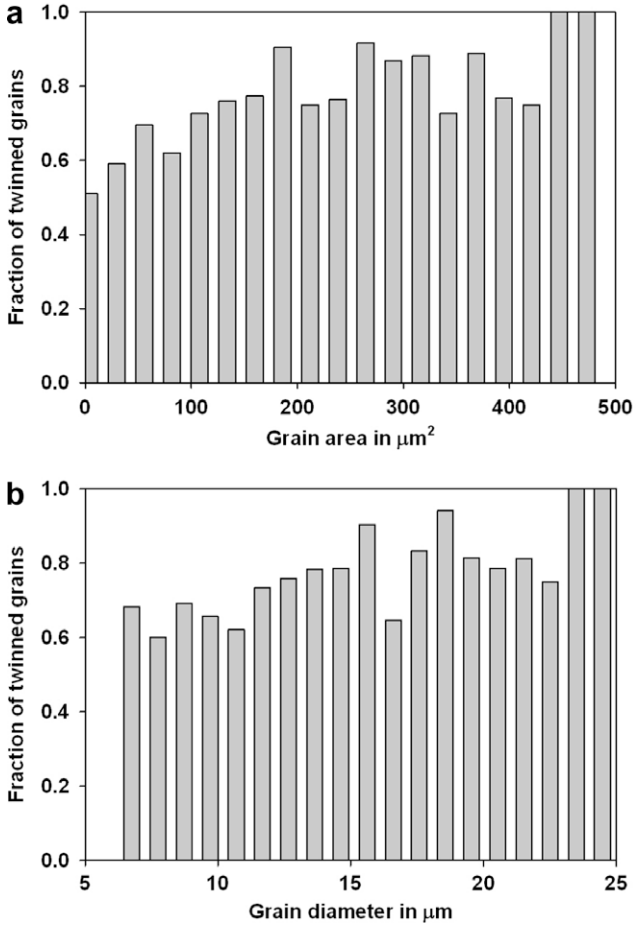

Fig. 10. The fraction of twinned grains as a function of: (a) grain area and (b) grain diameter.

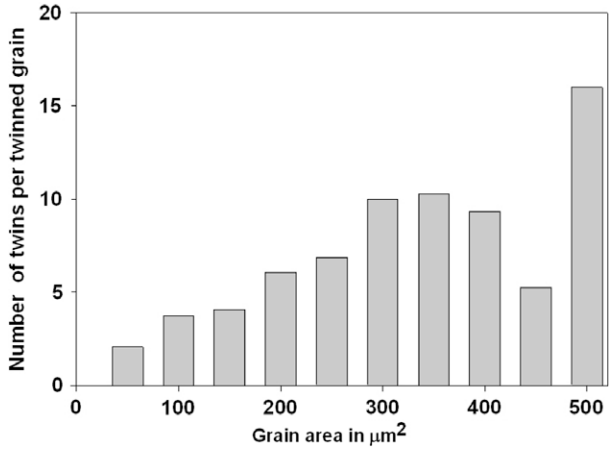

Fig. 11. The average number of twins per twinned grain is shown to increase with grain area.

respectively the change in twin thickness w and twin area fraction a_f per twinned grain with a given a_g. As shown, both quantities are independent of a_g according to our statistics. In addition, the average values that we calculate for w and a_f, considering only the grains that twinned, are 0.35 μm and 23%, respectively, for the 10% compressed sample. Similarly, a constant thickness for $\{10\bar{1}2\}$ twins has been reported elsewhere in single crystal [7] and polycrystalline [4] Zr.

The fact that w and a_f are both constant implies that the number of twins per twinned grain n increases proportionally with d_g, i.e., $n = kd_g$. The total twinned area per twinned grain follows $a_t \sim nwd_g \sim kwa_g$, and accordingly increases with a_g. The twin area fraction is $a_f = a_t/a_g \sim kw$ and thus remains constant and independent of a_g.

6. Discussion

Overall, 72.3% of all grains had twinned by 10% strain and these twinned grains were not limited to those that were preferentially oriented for twinning. A substantial fraction, 50%, of grains in the strongly textured material had $m_{(1)}$ greater than 0.37. Approximately 90% of these favorably oriented grains twinned by 10% strain. Yet, a large fraction of the less suitably oriented grains (with $m_{(1)}$ less than 0.37) have twinned, as can be seen in Fig. 3. Evidently both crystallographic conditions and local stress states are responsible for twinning.

Once twins have nucleated, twin growth was found to depend on orientation. For the 10% strained material, the twin thickness increased with the Schmid factor m. Although the actual resolved shear stress was not known, these results suggest that twin growth responds to the resolved shear stress induced by the externally applied load.

Grain area seemed to play a defining role in deformation twinning, provided that twin nucleation took place. For twinned grains, the number of twins n per grain was found to increase with grain area. However, whether a grain

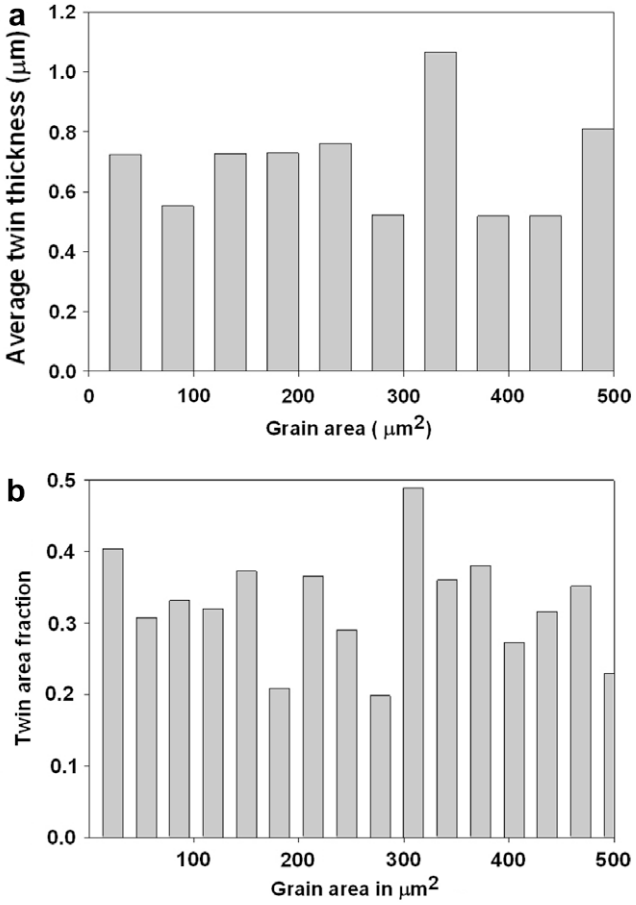

Fig. 12. (a) The average twin thickness per twinned grain and (b) the twin area fraction per twinned grain do not change with grain area.

twinned or not was weakly correlated with both grain area and with grain diameter. This means that small grains are almost as likely to contain at least one twin as large grains. Furthermore, we found that twin thickness and twin area fraction were more or less independent of grain area (Fig. 12).

There were two results from the present analysis that we found puzzling. First, little to no correlations were found between grain boundary misorientation angles larger than 5°, and twin nucleation or growth. Any slight preference was found for the smaller angles and may be explained by the transmission of the twin into a slightly misoriented neighbor. This result is surprising because larger stress gradients and stress concentrations (e.g., from pile-ups), which could drive twin formation, and higher densities of atomic- and nano-scale defects (e.g., ledges, excess volume, stacking faults), which would be excellent sources for twins, are usually associated with larger α. Perhaps a scalar measure of misorientation does not suffice to identify grain boundary structures that contain the defects needed for twin nucleation (if they exist). Nonetheless, the fact that α does not play a significant role in twinning implies that elastic anisotropy [33] and neighbor correlations may not be the most important characteristics to include in a twinning

model. Second, Fig. 6 shows that at 5% strain, the twin thickness w is independent of Schmid factor while at 10% strain, w increases with Schmid factor. We speculate that the former, less intuitive result, arises because of a back-stress acting on the twin domain due to the resistance in accommodating the twin shear by the surrounding grains. Twin growth is driven by a competition between the back-stress and the applied stress locally acting on the twin domain. As the flow stress increases with increasing strain, it becomes easier for the applied stress to overcome the backstress. Because, unlike the applied stress, the back-stress is relatively insensitive to orientation, it will be potentially easier for twins with higher Schmid factors to grow. Therefore at the lower 5% strain applied stresses may be comparable to the backstress, whereas at 10% strain, the applied stress contribution may exceed the backstress such that it can affect twin growth. Generally, when applied stress states can overcome the action of backstresses, a twin should be able to grow proportionally with resolved shear stress (up to the point of saturation). Generally, the magnitude of this backstress and how it would evolve with strain is unknown. In this regard, a recent study [34] measured the stress tensors in a twin and the matrix within a twinned Mg grain, found them to be very different, and confirmed the presence of the backstress. Following nucleation, the resolved shear stress on the twin had opposite sign than the average shear in the grain; and even after the twin had grown substantially (20% of the grain), the former resolved shear remained much smaller than the latter. This result may be attributed to backstresses.

The present results strongly suggest a need to change some ways twinning is modeled in constitutive descriptions for hcp metals. At present, the onset and growth of twinning is usually treated in a deterministic manner. For instance, only one variant per grain, the so called predominant twin system (PTS), is selected for re-orientation [2,3,12,17,35–37]. A CRSS is defined for twinning and therefore the PTS is the one with the largest resolved shear stress. The consequence of this approach is that all grains of similar orientation twin on the same (usually the first) variant. However, in this work, based on the relative orientation of the crystal and the macroscopic load direction, only a fraction of grains with similar orientation twinned. Moreover, the twin variant present was not always the one with the highest Schmid factor, only 60% were, and a non-negligible 21% of the observed twins corresponded to the variant with the second highest Schmid factor. This variation implies that the criterion for selecting which of the six variants needs to be based on a resolved shear stress that is determined from the stress tensor in the region of the twin rather than the geometric Schmid factors reported here. This local stress state that drives twin nucleation will include the mesoscopic deviations due to load sharing among the grains in the aggregate and the smaller scale (micro-scale down to atomic-scale) fluctuations due to the local surroundings. For the former, self consistent schemes, such as VPSC [38] and EPSC [39], calculate a uniform grain stress state that deviates from the applied state as a result of the anisotropy of the crystal and surrounding homogeneous effective medium. We already know that such an approach gives results which are consistent with the observed stress–strain and texture evolution in plastically deforming hcp metals [2,12,13,17,35]. The present results on twin thickness indicate that using only the average stress in the grain may be adequate for twin growth, since it is reasonable to expect that long-range stress fields are required to drive the twin across the grain.

The substantial statistical variation in the observed effects of crystallography and size suggest that for twin nucleation average stresses will not be sufficient. Both local stresses and smaller scale defects need to be considered in a probabilistic twin nucleation criterion. The local stresses responsible for twin nucleation are likely achieved through fluctuations present at very fine length scales (nanoscale and below). Therefore they cannot be directly related to mesoscale features of the microstructure such as grain orientation, grain boundary area, grain size, and grain boundary misorientation angle. Even if the length-scale and degree of these fluctuations were known and could be calculated, one cannot suppose that all stress concentrations lead to twinning. The twin nucleation criterion needs to additionally account for the probability that the critical (atomic-scale) defect for twinning is present [40]. While the present study is a mesoscopic treatment of twinning, the relationships between certain microstructural characteristics and twin activation and growth identified in this work have elucidated the importance of load stress and local defects, and ultimately can be used to guide and validate a probabilistic twinning model.

7. Conclusions

In this work, we performed a statistical analysis on large data sets collected from EBSD on high-purity polycrystalline zirconium (Zr) to examine the effects of several microstructural features on the likelihood that $\{10\bar{1}2\}$ twins nucleate and grow to sub-micron length-scales (where they become visible on an EBSD map). The microstructure features analyzed statistically were grain orientation (Schmid factor for twin), grain area, grain boundary misorientation angle α, prismatic slip activity (Schmid factor for prismatic slip systems) in a grain and neighboring grains.

In the present case in which strongly textured Zr was compressed at 77 K to induce twinning, whether a grain twins or not is related to the grain orientation with respect to the macro-stress. The fraction of grains that formed at least one twin increases with the maximum twin Schmid factor. Within the subset of grains that did twin, the twin variant with the highest Schmid factor has the highest probability of activation (56–60%), although the probability that other variants are activated is significant (21–23% for the second highest, 10% for the third). Therefore local stress variations with respect to the macroscopic stress play a secondary, but non-negligible role in twin variant selection.

The incidence of twinning is also found to be weakly dependent on grain area (or grain diameter). Small grains are nearly as likely to exhibit twins as large grains. Twin thickness, on the other hand, is relatively constant across the samples for a given strain level (0.25 μm for 5% and 0.35 μm for 10%) and insensitive to grain area, which explains why the twin area fraction in twinned grains was independent of grain area. Only among the subset of those grains in which twins formed do we find that the number of twins increases with grain size.

Finally, we find that neighbor misorientation angles larger than 5° only slightly affected twin nucleation (presence of twins or numbers of twins) and twin growth (twin thickness). Small preferences were observed for the smaller misorientation angles.

Acknowledgement

The authors would like to acknowledge support from the Office of Basic Energy Sciences, Project FWP 06SCPE401, under US DOE Contract No. W-7405-ENG-36.

References

[1] McCabe RJ, Cerreta EK, Misra A, Kaschner GC, Tomé CN. Philos Mag 2006;86:3595.
[2] Tomé CN, Maudlin PJ, Lebensohn RA, Kaschner GC. Acta Mater 2001;49:3085.
[3] Kaschner GC, Tomé CN, Beyerlein IJ, Vogel SC, Brown DW, McCabe RJ. Acta Mater 2006;54:2887.
[4] Reed-Hill RE. Role of deformation twinning in the plastic deformation of a polycrystalline anisotropic metal. Warrendale, PA: TMS; 1964.
[5] Partridge PG. Metall Rev 1967;12:168.
[6] Yoo MH, Lee JK. Philos Mag 1991;63:987.
[7] Rapperport EJ. Acta Metall 1959;7:254.
[8] Rapperport EJ, Hartley CS. Trans Am Inst Mining Metall Eng 1960;218:869.
[9] Akhtar A, Teghtsoonian A. Acta Metall 1971;19:655.
[10] Price PB. Proc Roy Soc Lond Ser A, Math Phys Sci 1961;260:251.
[11] Capolungo L, Beyerlein IJ, Tomé CN. Scripta Mater 2009;60:32.
[12] Proust G, Tomé CN, Kaschner GC. Acta Mater 2007;55:2137.
[13] Capolungo L, Beyerlein IJ, Kaschner GC, Tome CN. Mater Sci Eng A 2009;513–514:42.
[14] Serra A, Bacon DJ, Pond RC. Acta Mater 1999;47:1425.
[15] McCabe RJ, Gnl Proust, Cerreta EK, Misra A. Int J Plast 2009;25:454.
[16] Marshall P, Proust G, Rogers JT, McCabe RJ. J Microsc; accepted for publication.
[17] Beyerlein IJ, Tomé CN. Int J Plast 2008;24:867.
[18] Capolungo L, Beyerlein IJ. Phys Rev B 2008;78:024117.
[19] Mendelson S. Mater Sci Eng 1969;4:231.
[20] Mendelson S. J Appl Phys 1970;41:1893.
[21] Serra A, Bacon DJ. Philos Mag 1996;73:333.
[22] Yoo MH. Trans Metall Soc AIME 1969;245:2051.
[23] Song SG, Gray GT. Acta Metall Mater 1995;43:2325.
[24] Meyers MA, Vohringer O, Lubarda VA. Acta Mater 2001;49:4025.
[25] Hull D. Acta Metall 1961;9:191.
[26] Christian JW, Mahajan S. Prog Mater Sci 1995;39:1.
[27] Barnett MR, Keshavarz Z, Beer AG, Atwell D. Acta Mater 2004;52:5093.
[28] Armstrong R, Codd I, Douthwaite RM, Petch NJ. Philos Mag 1962;7:45.
[29] Chun JS, Byrne JG, Borneman A. Philos Mag 1969;20:291.
[30] Okazaki K, Conrad H. Acta Metall 1973;21:1117.
[31] Hosford WF. The mechanics of crystals and textured polycrystals. New York: Oxford University Press; 1993.
[32] Barnett MR. Scripta Mater 2008;59:696.
[33] Yoo MH, Morris JR, Ho KM, Agnew SR. Metall Mater Trans A 2002;33:813.
[34] Aydiner CC, Bernier JV, Clausen B, Lienert B, Tomé CN. Phys Rev B; accepted for publication.
[35] Brown DW, Sisneros TA, Clausen B, Abeln S, Tomé CN, Vogel SC, et al.; in preparation.
[36] Proust G, Tomé CN, Jain A, Agnew SR. Int J Plast 2009;25:861.
[37] Tomé CN, Lebensohn RA, Kocks UF. Acta Metall Mater 1991;39:2667.
[38] Lebensohn RA, Tome CN. Acta Metall Mater 1993;41:2611.
[39] Clausen B, Tomé CN, Brown DW, Agnew SR. Acta Mater 2008;56:2456.
[40] Wang GJ, Hoagland R, Hirth JP, Capolungo L, Beyerlein IJ, Tomé CN. Scripta Mater 2009;61:903.